Twisted Perylene Diimides with Tunable Redox Properties for Organic Sodium-Ion Batteries

6 authors, including:

Harish Banda
Massachusetts Institute of Technology
16 PUBLICATIONS   **698** CITATIONS

SEE PROFILE

Dijo Damien
Christ College, Irinjalakuda
20 PUBLICATIONS   **1,214** CITATIONS

SEE PROFILE

Kalaivanan Nagarajan
University of Strasbourg
33 PUBLICATIONS   **1,509** CITATIONS

SEE PROFILE

Ashish Raj
Université Catholique de Louvain - UCLouvain
7 PUBLICATIONS   **67** CITATIONS

SEE PROFILE

Some of the authors of this publication are also working on these related projects:

Project   Strategies to reduce the rate of charge recombination View project

Project   Organic Batteries View project

FULL PAPER

Sodium-Ion Batteries

ADVANCED
ENERGY
MATERIALS

www.advenergymat.de

Twisted Perylene Diimides with Tunable Redox Properties for Organic Sodium-Ion Batteries

Harish Banda, Dijo Damien, Kalaivanan Nagarajan, Ashish Raj, Mahesh Hariharan,* and Manikoth M. Shaijumon*

Organic rechargeable batteries gain huge scientific interest owing to the design flexibility and resource renewability of the active materials. However, the low reduction potentials still remain a challenge to compete with the inorganic cathodes. This study demonstrates a simple and efficient approach to tune the redox properties of perylene diimides (PDIs) as high voltage cathodes for organic-based sodium-ion batteries (SIBs). With appropriate electron-withdrawing groups as substituents on perylene diimides, this study shows a remarkable tunability in the discharge potential from 2.1 to 2.6 V versus Na$^+$/Na with a sodium intake of ≈1.6 ions per molecule. Further, this study explores tuning the shape of the voltage profiles by systematically tuning the dihedral angle in the perylene ring and demonstrates a single plateau discharge profile for tetrabromo-substituted perylene diimide (dihedral angles θ_1 & θ_2 = 38°). Detailed structural analysis and electrochemical studies on substituted PDIs unveil the correlation between molecular structure and voltage profile. The results are promising and offer new avenues to tailor the redox properties of organic electrodes, a step closer toward the realization of greener and sustainable electrochemical storage devices.

1. Introduction

Sodium ion batteries (SIBs) have been extensively studied in the recent past as an alternative to their lithium counterparts (LIBs), owing to concerns regarding cost and limited reserves of lithium. Particularly, in large-scale storage applications like hybrid vehicles and renewable power stations, SIBs, with the abundance and low cost of sodium, are more viable than LIBs.[1–6] Sodium exhibits electrochemical properties similar to that of lithium (0.3 V more positive) and its ionic radius is about 1.3 times to that of lithium ion. While the positive

potential offers better safety, it also lowers the reduction potential of the active materials.[7,8] Recently, several transition metal-based systems have been proposed as promising electrode materials for SIBs,[3,4] but high production costs and the associated environmental concerns question the long-term reliance on these materials. Also, the insertion of large Na$^+$ ions into rigid lattices results in multistep phase transitions and the materials often suffer from low capacity utilization or sluggish kinetics.[8,9]

Organic materials with promising features like light weight, design flexibility at the molecular level, good resource renewability and low production costs are emerging as promising alternatives to inorganic materials.[10–12] Recent reviews on organic materials show significant developments on radical and carbonyl based materials for batteries.[13,14] However, the low reduction potentials offered by these materials compared to their inorganic counterparts outweigh all the merits.[15–17] With the inherent 0.3 V more positive reduction potential of Na than Li, it is even more challenging to achieve higher reduction potentials with organic materials for SIBs. Radical based materials offer the highest reduction potentials among organic materials for SIBs, but they depend on large anions like PF$_6^-$ and ClO$_4^-$ for charge compensation.[8,9] These large electrolyte anions cannot be readily inserted into active material and require large amounts of electrolyte while compromising the practical specific energy densities.[15,18] Carbonyl compounds, particularly carboxylate salts and anhydride-based materials, with their great diversity, can be tailored for desired properties.[19–23]

Redox potential of a molecule can be tailored by tuning its highest occupied molecular orbital (HOMO) and lowest occupied molecular orbital (LUMO) energy levels. According to the molecular orbital theory, a lower LUMO level means higher electron affinity and thus a higher reduction potential for the molecule. Lowering the LUMO levels could be achieved in two ways. Attaching electron withdrawing groups to the redox active molecule is one way[15,24–27] and extending the conjugation in a molecule through aromatic rings is another conventional way.[10,21,28] Extending the conjugation could increase the electrochemical dead weight of the molecule and result in reduced theoretical capacity. Nevertheless, extended conjugation is expected to increase the ion intake and practical capacity of a

H. Banda,[+] Dr. D. Damien, Dr. K. Nagarajan, Prof. M. Hariharan
School of Chemistry
Indian Institute of Science Education and Research
Thiruvananthapuram 695016, Kerala, India
E-mail: mahesh@iisertvm.ac.in
H. Banda, Dr. D. Damien, A. Raj, Prof. M. M. Shaijumon
School of Physics
Indian Institute of Science Education and Research
Thiruvananthapuram 695016, Kerala, India
E-mail: shaiju@iisertvm.ac.in

[+]Present address: SyMMES, INAC, CEA, F-38000 Grenoble, France

The ORCID identification number(s) for the author(s) of this article can be found under https://doi.org/10.1002/aenm.201701316.

ADVANCED
SCIENCE NEWS
www.advancedsciencenews.com

ADVANCED
ENERGY
MATERIALS
www.advenergymat.de

molecule. A recent report demonstrates this in sodium stilbene dicarboxylate (SSDC).[21] SSDC shows a discharge capacity of 222 mA h g^{-1} whereas its lower ring counterpart, sodium benzene dicarboxylate (SBSC) shows 162 mA h g^{-1}.

Extended conjugation reduces the HOMO–LUMO gap (E_g) in a molecule and offers better electronic conduction and a lower degree of polarization.[10] This results in better redox reversibility and, thus, delivers practical capacities close to the theoretical value.

Recently, Dunn and co-workers have demonstrated the effect of substitution on electrochemical performance of naphthalene diimides for LIBs.[15] While they could achieve higher reduction potentials with some derivatives, unfortunately, the reversible discharge capacities were less than half of the theoretical capacities in most cases. Only very few reports are focused on tuning organic materials to offer high reduction potentials for LIBs.[26,28–30] Though the knowledge of Li electrochemistry is expected to be applicable for sodium as well, at times, latter behaves in a dissimilar fashion and investigations are yet to address this anomaly.[31–34] Kim et al. made the first and only attempt to tune the redox potential by employing halogen- substituted quinone derivatives as cathode materials for SIBs, but with poor cyclability.[35] However, none of these reports discuss the energetic structure–voltage profile correlation. Considering all the concerns mentioned above and benefitting from the vast synthesis knowledge available in the literature, we opted to study the effect of substituting electron

withdrawing groups on N,N′-bis(n-propylacetyl)-perylene-3,4,9,10-tetracarboxylic diimide (PDI) in SIBs. PDI is an excellent canvas to portray tailoring of redox potentials, as it possesses an extended conjugation over two naphthalene subunits and offers four bay positions and 4 ortho positions for substitutions. Detailed structural analysis and electrochemical studies on substituted PDIs shed light on correlation between molecular structure and voltage profile. Through an understanding of the effect of twist in the perylene ring, we could successfully tailor the shape of voltage profile to a single plateau. Our report is an interesting case study of tuning the shape of voltage profile and is the first report of its kind in organic literature for both SIBs and LIBs.

2. Results and Discussion

The experimental evaluation of the effect of electron-withdrawing groups on electrochemical performance was performed through synthesis of various perylene diimide derivatives by following **Scheme 1**, starting from perylene-3, 4,9,10-tetracarboxylic acid (PTCDA). The synthesized derivatives, with good solubility in common solvents, were characterized through various spectroscopic techniques (see synthesis and characterization section in Supporting Information). **1** was synthesized from PTCDA through the conventional imidization
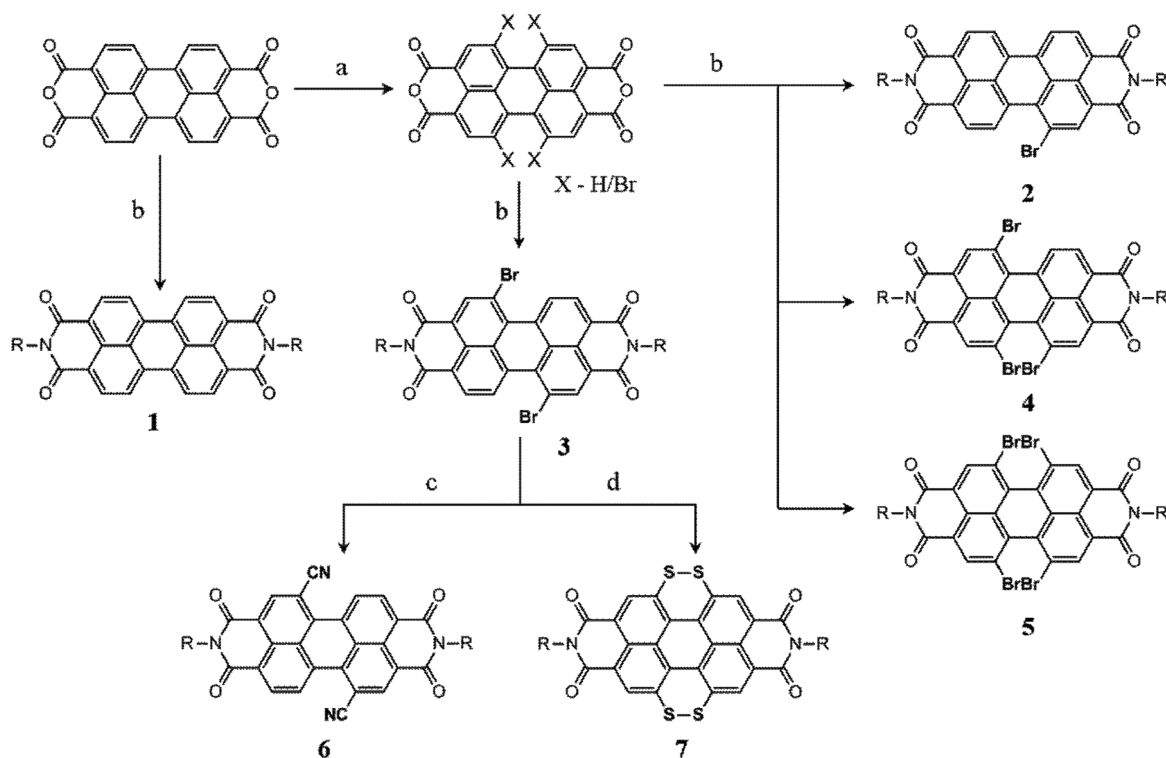
PDI	PDI-Br	PDI-Br$_2$	PDI-Br$_3$	PDI-Br$_4$	PDI-CN$_2$	PDI-S$_4$
1	2	3	4	5	6	7

Scheme 1. Synthesis of perylene diimide derivatives a) Br$_2$, I$_2$, H$_2$SO$_4$, 85 °C, b) 3-amino-1-propanol, DMA, 1,4-dioxane, 110 °C; Acetic anhydride, Pyridine, RT, c) CuCN, DMF, 150 °C, d) CH$_3$COSK, CH$_3$OH, CHCl$_3$. (R: n-propyl acetate).

**ADVANCED
SCIENCE NEWS**
www.advancedsciencenews.com

**ADVANCED
ENERGY
MATERIALS**
www.advenergymat.de

process with a yield of 50%. **3** was synthesized with a yield of 70% by following a two-step procedure of bromination and imidization on PTCDA.[36] Cyanation of **3** was performed through a reported procedure and **6** was obtained in 59% yield.[37] Electrochemical performance of the synthesized derivatives was analyzed through cyclic voltammetry and galvanostatic cycling measurements. Cyclic voltammetry was performed to test the reversible ingress of sodium ions and two pairs of broad reversible redox peaks were observed in **1**, **3**, and **6** (Figure S1, Supporting Information). Differential capacity plots (voltage vs. dQ/dE),[38] obtained through the galvanostatic charge–discharge measurements, show two sets of relatively sharp redox peaks at 2.2 and 1.7 V for **1**, which correspond to the formation of radical anion and dianion, respectively (**Figure 1**a).[39] As expected with the increase in electronegativity, both the substituted derivatives viz. **3** and **6**, show a shift in the first and second redox potentials toward higher voltages when compared to **1**. **6** shows a greater potential than **3** with cyanide being a better electron-withdrawing group than bromine.

The first reduction of **6** occurs at about 340 mV greater than **3** and 450 mV greater than **1**.

Redox behavior of perylene-based systems as diimides,[39] anhydrides,[31] and polyimides[32,40,41] have been studied extensively in the literature and all the reports suggest a two-step reduction process with formation of radical anion as an intermediate. The redox processes are associated with the conversion of carbonyl groups in the imide ring to enolate functionality. Recently, Wurthner and co-workers successfully synthesized the first ambient stable derivatives of perylene diimide radical anion and dianion and could completely characterize the two species, otherwise unstable.[42,43] With the synthesized sodium salt of dianion species, the coordination between sodium ions and the enolate functionality could be successfully demonstrated. Figure 1b shows the electrochemical redox mechanism of sodium ion insertion and de-insertion for perylene diimides during the charge–discharge processes.

To establish a correspondence between the reduction potentials and the electron-withdrawing ability of the substituents, energy levels of the derivatives were analyzed. LUMO energy levels, which are known to directly correlate to the reduction potentials of the species,[10] were calculated for the derivatives in their gaseous phase using B3LYP/6-311+G(d, p) level of theory. The LUMO energy values obtained for the PDI derivatives span from −4.6 eV for the highly electron deficient **6** to −4.0 eV for the unsubstituted **1** with an intermediate value of −4.1 eV for moderately electron deficient **3**. The first reduction potentials observed in the differential capacity plots show a linear relationship with the calculated LUMO energy values (Figure 1c), thus, correlating the electron-withdrawing ability of substituents to the reduction potentials of the derivative. This excellent equivalence between theory and experimental results highlight the level of flexibility organic molecules offer in tailoring the materials for desired properties.

Having analyzed the redox properties of PDI derivatives, we carried out the galvanostatic charge–discharge cycling to estimate their sodium ion storage capabilities (Figure 1d). All the derivatives show a two plateau voltage profile with the plateaus being quite consistent with the redox peaks observed in the
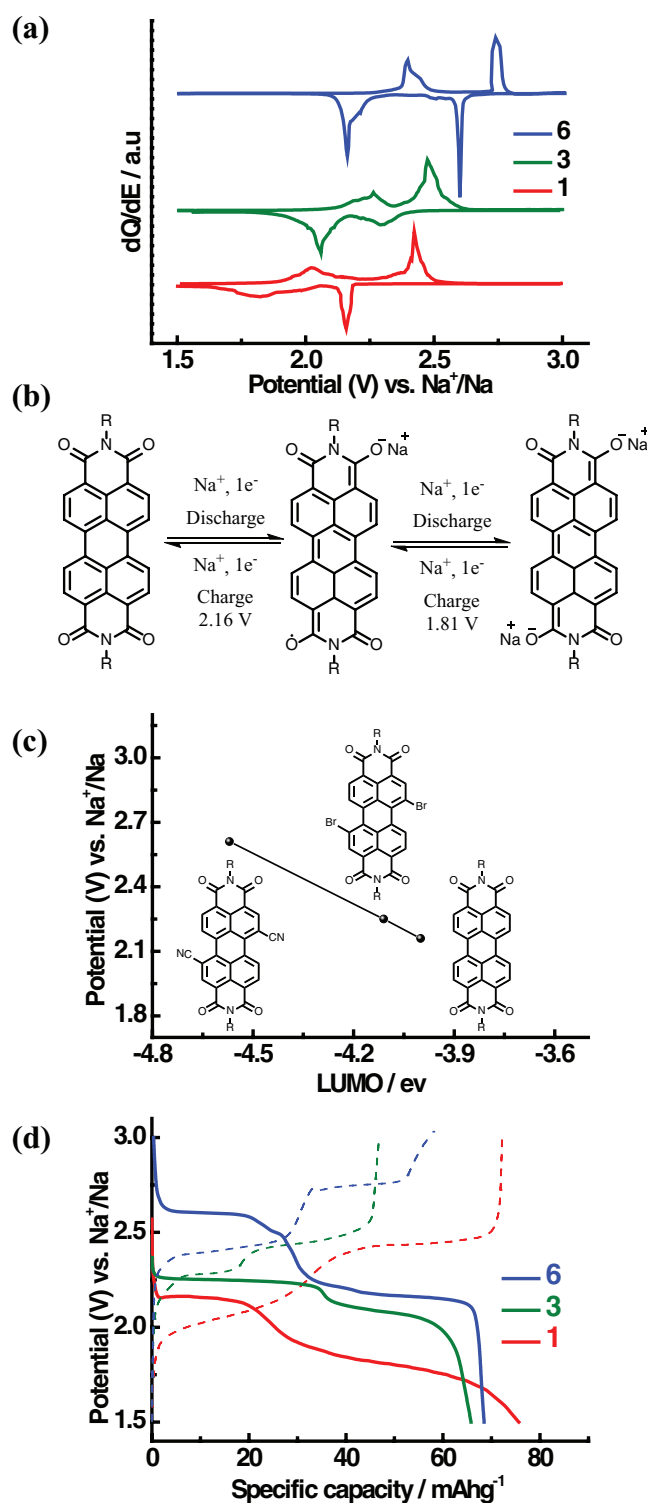
Figure 1. a) Differential capacity plots of **1**, **3**, and **6** cycled at a current rate of C/4 in voltage ranges between 1.5 and 3.0 V versus Na$^+$/Na. b) Schematic representation of the charge–discharge mechanism for the perylene diimide derivatives. c) First reduction potential versus calculated LUMO energy levels for **1**, **3**, and **6**. d) Charge–discharge voltage profiles of **1**, **3**, and **6** cycled at a current rate of C/4. A systematic shift in the voltage profile toward higher redox potentials can be noted from **1** to **3** and **6**. Cyanide being a better electron-withdrawing group results in higher potentials for **6** than the bromine substituted **3**.

**ADVANCED
SCIENCE NEWS**
www.advancedsciencenews.com

**ADVANCED
ENERGY
MATERIALS**
www.advenergymat.de

Table 1. Galvanostatic cyclic performance of 1, 3, and 6.

Label	Theoretical capacity (2e⁻) [mA h g⁻¹]	Experimental capacity[a] @ 20 mAg⁻¹ [mA h g⁻¹]	Na⁺ intake per molecule	LUMO[b] [eV]	First reduction potential[c] [V vs Na⁺/Na]
1	91	77	1.68	−4.0	2.16
3	71	66	1.83	−4.1	2.27
6	84	64	1.62	−4.6	2.61

[a]The first discharge capacity observed when cycled at a current density of 20 mAg⁻¹ in voltage ranges between 1.5 and 3.0 V versus Na⁺/Na; [b]Gas-phase values obtained with the B3LYP/6-311+ G(d, p) level of theory; [c]The first reduction peak potential observed from differential capacity plots plateau when cycled at a current density of 20 mAg⁻¹ in voltage ranges between 1.5 and 3.0 V versus Na⁺/Na.

respective CVs. A systematic lift in the voltage profiles can be noticed from **1** to **3** and **6**. Further, all the derivatives demonstrate first discharge capacities near to that of the theoretical capacities calculated for a two electron redox process (**Table 1**). The near theoretical capacities are expected with an extended conjugation over the two naphthalene rings in PDI as opposed to less than half utilization seen in naphthalene diimides for LIBs.[15] Further, unlike the substituted naphthalene diimides for LIBs, herein, being a cathode material, it is highly desirable to galvanostatically cycle at higher electrochemical window.

PDI derivatives in the present study are cycled at a higher potential window of 1.5–3.0 V versus Na⁺/Na opposed to 1.0–4.0 V versus Li⁺/Li for naphthalene diimides for LIBs.[15] **1**, **3**, and **6** show discharge capacities of 74, 66, and 64 mA h g⁻¹, respectively, which suggest a sodium ion intake of 1.6 to 1.8 per molecule. Figure S2 (Supporting Information) shows the voltage profiles illustrating sodium ion intake per molecule during the charge–discharge process.
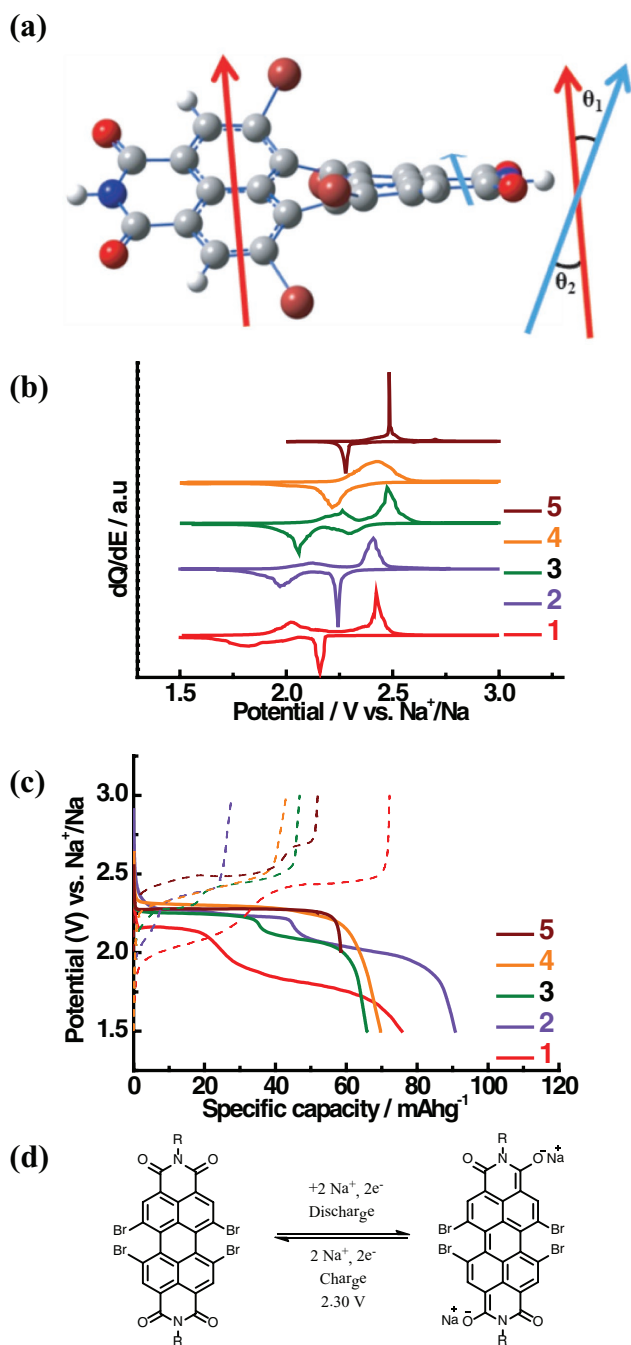
Although the synthesized derivatives demonstrate good sodium ion intake in the first discharge, a clear drop in the charge and discharge capacities could be spotted thereafter (Figure S2, Supporting Information). Regardless of the drop in capacities, the redox plateaus for first charge and the second cycles still occur at potentials corresponding to peaks observed in the respective CVs, excluding the possibility of irreversibility. Hence, the drop in capacities is attributed to the fact that the synthesized derivatives are highly soluble in the electrolyte and will dissolve during cycling. Also, low capacities obtained for the derivatives are understandable with the presence of bulky imide side chains. Polymerization has been demonstrated as an efficient technique in circumventing these challenges.[32] Further, polymerization through hydrazine as a linker is reported as an excellent technique which will not add any extra weight to the molecule but significantly enhances the specific capacities and the overall electrochemical performance of perylene diimides.[32,40] Apart from altering the HOMO–LUMO levels of the molecule, the added substituents also induce a twist in the perylene ring. In order to avoid electrostatic repulsions between the substituents and the hydrogen atoms on opposite bay positions, the perylene ring stabilizes into a twisted geometry. The two dihedral angles between the naphthalene subunits depend upon the extent of electrostatic repulsions. A schematic of the dihedral angles formed between the naphthalene subunits in a perylene ring is shown in **Figure 2**a. 1 has a planar structure with zero dihedral angles whereas **3** shows about 23° for both θ_1 and θ_2. Changes in the dihedral angles of a neutral PDI derivative will also affect the relative energies of its reduced forms

(radical anion and dianion). Recently, Wurthner and co-workers reported that, the changes in the relative energies of radical anion and dianion alter the redox potentials of quinones and perylene diimides.[43] They performed solvent-dependent cyclic voltammetric study on substituted perylene diimide derivatives to analyze the solvent dependency of the redox properties of its radical anion and dianion.[43] With increasing polarity, the two reduction peaks are noted to move closer and eventually merge into a single peak in a highly polar solvent, such as methanol. They propose that this could be due to a preferential formation of the dianion species over radical anion owing to a superior stabilization of dianion via hydrogen bonding with increasing polarity. A single redox peak meant a complete preference for formation of dianion over the radical anion. The equilibrium constants determined for the disproportionation reaction of radical anion resulting in neutral and dianion species support this argument.

Achieving a single plateau in voltage profile for rechargeable battery electrodes is very important, and could be accomplished in organic-based electrodes either by means of molecular design or by deploying different electrolytes. Here we attempted to tune the molecular design to obtain a single plateau in the voltage profile, as the latter option might lead to electrolyte compatibility issues. Similar to earlier approach, instead of changing the polarity of solvent to tune the energy levels of reduced species, we presumed that introducing a systematic twist into the perylene ring would have a similar influence. To test the feasibility of this approach, change in Gibbs free energies (ΔG) was calculated for the formation of reduced species in a series of bromo-substituted PDIs (**2-5**) in their gaseous states using B3LYP/6-311+G (d, p) level of theory.

Bromine derivatives were chosen considering the facile synthesis procedures necessary for the eventual experimental study. Figure S3 (Supporting Information) shows an energy-level diagram with ΔG for the formation of radical anion and dianion for PDI and its bromo-substituted derivatives. While **1–3** show a greater preference for formation of a radical anion, **4** and **5** favor formation of dianion species as evidenced from the ΔG values consolidated in Table S2 (Supporting Information). Thus, the preference toward direct formation of a dianion species could result in a single redox process rather than a two-step redox process. The greater ΔG values for dianion formation in **4** and **5** could, hence, result in higher reduction potentials and better feasibility of the reduction process compared to **1–3**.

Motivated by these encouraging theoretical findings, we synthesized a class of PDI bromo derivatives (**2–5**) in order to systematically analyze the effect of dihedral angles on the
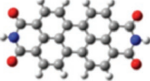
ADVANCED
SCIENCE NEWS
www.advancedsciencenews.com

ADVANCED
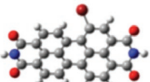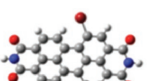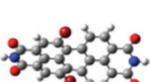**ENERGY**
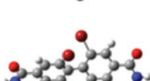**MATERIALS**
www.advenergymat.de

Figure 2. a) Schematic depiction of the two dihedral angles, which vary with respect to the substituents on the bay positions of perylene moiety, b) differential capacity plot, and c) charge–discharge voltage profiles of 1–5 cycled at a current rate of C/4 in voltage ranges between 1.5 and 3.0 V versus Na$^+$/Na. d) Schematic representation of the charge–discharge mechanism for 5. The two plateaus shift closer with increasing dihedral angles for 1–3 and eventually appear as single plateau in 4 and 5.

redox properties of PDI. Spectroscopic characterization of all the derivatives can be found in Supporting Information. The dihedral angles obtained through optimized structures show a gradual increase in θ_1 and θ_2 from 1 to 5 (Table 2). Cyclic voltammetry was performed to verify the reversible

ingress of sodium ions into the synthesized derivatives (Figure S4, Supporting Information). The broad reduction/oxidation peaks observed in all the derivatives are found to be reversible. To analyze the peak potentials accurately, differential capacity plots were obtained through galvanostatic cycling. Two redox pairs for 1, 2, and 3, a single broad redox pair in 4 and a single sharp redox pair for 5 were observed (Figure 2b). A gradual decrease in the peak separation (δP) between first reduction and second reduction can be clearly noted for derivatives from 1 to 3. δP decreases from 524 mV in 1 to 302 mV in 2 and 242 mV in 3 beyond which the peaks merge and appear as a broad peak in 4 and as a single sharp peak in 5 (Table 2). These findings are in excellent agreement with the trend observed in solvent dependent cyclic voltammograms studied in the earlier report.[43] 4 and 5, as observed in the ΔG values, show a better reduction potential than 1–3, which is attributed to the proportional increase in the cell potential with the change in free energy. Charge–discharge voltage profiles were obtained for 1–5 through galvanostatic cycling in the voltage range of 1.5–3.0 V for 1–4 and 2.0–3.0 V for 5 versus Na$^+$/Na at a current rate of C/4 (Figure 2c). A gradual change in the shape of the voltage profiles of 1 to 5 can be noted. The two well-separated discharge plateaus move closer from 1 to 3 and eventually merge and give rise to a single plateau in 4 and 5. Also, all the derivatives deliver practical capacities close to the calculated theoretical capacities with a sodium ion intake greater than 1.7 per molecule in all derivatives (Table 2). Figure S5 (Supporting Information) illustrates the voltage profiles for 1–5 with sodium ion intake per molecule during the charge–discharge process. A perfect single plateau voltage profile with a practical discharge capacity corresponding to 98% of the theoretical capacity could be obtained for 5 (Figure S5e, Supporting Information). The practical capacities corresponding to almost two sodium ion insertion along with the single redox pair obtained from discharge capacity plots led us to predict a single step redox mechanism for 5 as shown in Figure 2d. The proposed mechanism corroborates with the theoretical calculations and the report in literature on solvent dependent cyclic voltammetry for perylene diimides.[43]

Further, we synthesized a control derivative that has four substituents on its four bay positions and yet has a near planar perylene ring in order to confirm hypothesis on the relation between dihedral angles and shape of voltage profile. N,N′-bis(n-propylacetyl)-1,6,7,12-bis-dithiano-perylene-3,4,9,10-tetracarboxylic diimide (7), which has all its bay positions substituted by sulfur moiety, still retains its planar structure of the perylene ring. Synthesis of 7 is accomplished by following a reported procedure[44] (Scheme 1) and the obtained crystal structure (Table S2, Supporting Information) shows ≈6° dihedral angles for both θ_1 and θ_2 (Figure S6, Supporting Information). A two-step voltage profile is expected for 7 owing to the near planar geometry of its perylene ring. As expected, differential capacity plot shows two pairs of broad reversible redox peaks (**Figure 3**a) and, correspondingly, two sloped plateaus are spotted in the charge–discharge voltage profiles (Figure 3b). The two redox peaks could be attributed to the formation of radical anion and dianion as reported earlier. The obtained results are in accordance with our prediction of two plateaus for a planar

Table 2. Comparison of the electrochemical performance of 1–5 corresponding to the respective dihedral angles.

Compound	Label	Theoretical capacity (2e) [mA h g^{-1}]	Experimental capacity [mA h g^{-1}] @ 20 mAg^{-1}	Na$^+$ intake per molecule	First reduction potential [V vs Na$^+$/Na]$^{a)}$	θ_1 [°]	θ_2 [°]	Reduction peak separation$^{b)}$ [mV]
	1	91	77	1.68	2.16	0	0	524
	2	80	90	2.25	2.24	23	4	302
	3	71	66	1.83	2.25	23	23	242
	4	65	69	2.15	2.28	24	38	–
	5	59	58	1.98	2.29	36	38	–

$^{a)}$The average value observed for the first reduction plateau when cycled at 20 mAg^{-1}; $^{b)}$The separation between reduction peaks observed in the cyclic voltammograms when scanned in the voltage ranges between 1.5 and 3.0 V versus Na$^+$/Na at a scan rate 0.1 mVs^{-1}. Dihedral angles are obtained from the optimized geometries using B3LYP/6-311+G (d, p) level of theory.
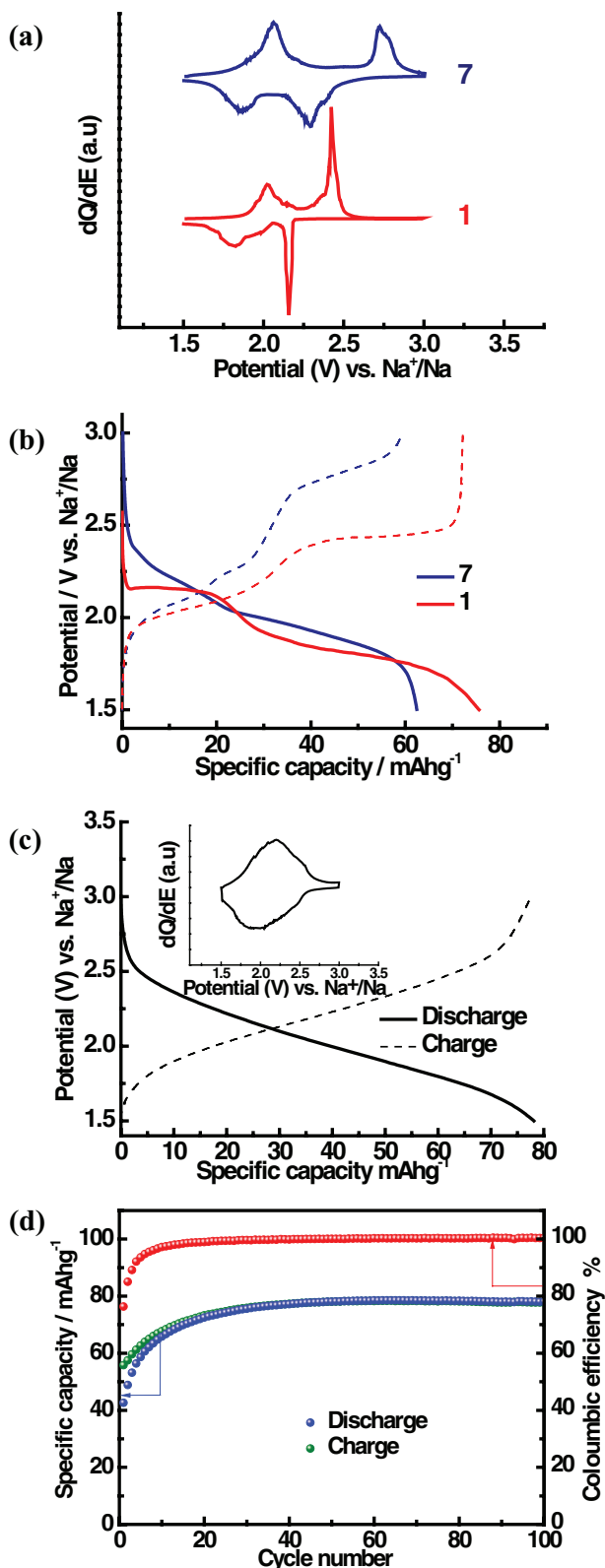
perylene ring and reinforce our concept of tuning the shape of voltage profile with dihedral angle.

However, a clear drop in the charge and discharge capacities could also be spotted in all the bromine derivatives (**2–5**) right after the first discharge process (Figure S5e, Supporting Information). Scanning electron microscopy (SEM) images obtained from electrodes before and after cycling show a clear loss of active material (Figure S7, Supporting Information). Finally, we demonstrate polymerization as an efficient technique to prevent dissolution of electrode materials and offer good cyclic stabilities for the synthesized derivatives.[45–47] Among the various synthesized derivatives, **4** and **5** demonstrate single plateau profiles whereas others show two-step profiles. Further, **4** offers a theoretical discharge capacity of 68 mA h g^{-1} while **5** offers 58 mA h g^{-1}. In order to demonstrate good cycling behavior with a better discharge capacity and a one-step discharge profile, we chose to polymerize **4**. **4** is first converted to an anhydride and then polymerized with hydrazine hydrate following **Scheme 2** to give N,N′-diamino-1,6,7-tribromo-perylene-3,4,9,10-tetracarboxylic polyimide (**8**). SEM images and UV–vis spectroscopy were performed to compare **4** and **8** and observe the insolubility of **8** (Figure S8, Supporting Information). Galvanostatic cycling was performed at a current rate of C/4 in the voltage range of 1.5–3.0 V versus Na$^+$/Na to study the electrochemical performance of **8**. The differential capacity plot in the inset of Figure 3c shows a single broad redox pair corresponding to a sloped plateau observed in the voltage profile in Figure 3c. Being a polymer, **8** delivered a remarkably stable practical capacity of 78 mA h g^{-1}, close to the calculated theoretical capacity of 84 mA h g^{-1}, over hundred cycles (Figure 3d). Cyclic stability and rate capability studies of
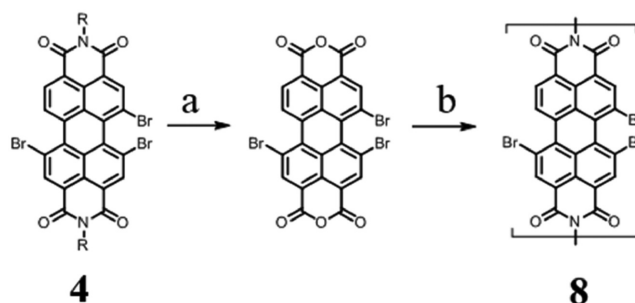
4 and **8** also further highlight the advantages of polymerization (Figure S9, Supporting Information). Although demonstrated only with **4**, polymerization could be extended to other diimides derivatives as an excellent strategy to avoid electrode dissolution and achieve good cyclic stabilities. Further, a gradual increase in capacity for about 20 cycles to the stable capacity is noted. This behavior is generally attributed to electrode activation during cycling by formation of new electronic and ionic conducting pathways during cycling. Electrochemical impedance spectroscopy was performed before and after 40 charge–discharge cycles to understand this. The Nyquist plots and corresponding equivalent circuits (Figure S10, Supporting Information) show high charge transfer and bulk resistance of 2194 Ω before cycling and a reduced value of 526 Ω after 40 cycles. This confirms the activation process during the initial cycles.

3. Conclusions

In summary, we have demonstrated an efficient approach to tune the reduction potentials and voltage profiles of perylene diimide-based organic electrodes for SIBs by substitution of electron-withdrawing groups. Cyano-substituted perylene diimide (**6**) shows an increase of 450 mV over its unsubstituted counterpart. Also, the synthesized derivatives offered a high sodium ion intake of 1.6–1.8 per molecule. Further, we also report the first study on tuning the shape of the voltage profiles of an organic material, by inducing a systematic twist into the perylene ring. Tetra bromo-substituted perylene diimide, with dihedral angles of 38° each, demonstrates a straight single plateau discharge profile. A control derivative

**ADVANCED
SCIENCE NEWS**
www.advancedsciencenews.com

**ADVANCED
ENERGY
MATERIALS**
www.advenergymat.de

Scheme 2. Synthesis of tri-bromo perylene diimide polyimide. a) KOH, *t*-BuOH reflux 2 h, b) Hydrazine hydrate, NMP reflux 6 h. (R: n-propyl acetate).

(**7**) with nearly planar ring geometry, despite of having four bay substituents, was synthesized to support the proposed hypothesis. Finally, tri bromo-substituted perylene polyimide (**8**) was synthesized to demonstrate polymerization as an efficient technique to achieve good cyclic stability with all the derivatives. **8** delivers a stable practical capacity of 78 mA h g^{-1} close to its theoretical capacity of 86 mA h g^{-1}. PDI derivatives with low weight substituents, for example, tetracyano-substituted perylene polyimide (PI-CN$_4$), could deliver much higher capacities, comparable to the current inorganic materials, with a single plateau discharge profile. We believe that the current study will offer new avenues to tailor the redox properties of organic materials as electrodes for rechargeable organic sodium ion batteries.

4. Experimental Section

Material Synthesis: *N,N′*-bis(*n*-propylacetyl)-perylene-3,4,9,10-tetracarboxylic diimide (**1**) was synthesized as a control derivative while *N,N′*-bis(*n*-propylacetyl)-1,7-dibromoperylene-3,4,9,10-tetracarboxylic diimide (**3**) and *N,N′*-bis(*n*-propylacetyl)-1,7-dicyanoperylene-3,4,9,10-tetracarboxylic diimide (**6**) were synthesized to demonstrate the effect of electron-withdrawing groups on PDI. Further, to understand the effect of twist generated by substituents on the perylene ring, a range of bromine derivatives (**2–5**) and *N,N′*-bis(*n*-propylacetyl)-1,6,7,12-bis-dithiano-perylene-3,4,9,10-tetracarboxylic diimide (**7**) were synthesized. Considering that all the diimides mentioned above face serious dissolution problem, *N,N′*-diamino-1,6,7-tribromo-perylene-3,4,9,10-tetracarboxylic polyimide (**8**) is designed as a model to demonstrate polymerization as an efficient strategy to achieve good cyclic stability. This strategy can be extended to other diimides to achieve the desired electrochemical properties. All the perylene diimide derivatives studied in this work were synthesized by procedures shown in Schemes 1 and 2. Details of the synthesis protocols and characterization through standard spectroscopic techniques for all the derivatives are available in the Supporting Information.

Materials Characterization: Fourier transform infrared spectra (FT-IR) were recorded on a Shimadzu IR Prestige-21 FT-IR spectrometer with KBr pellets. CHN analysis was carried out on an Elementary vario MICRO cube elemental analyzer. Thermo gravimetric analysis (TGA) was performed using a SDT Q600 Thermo gravimetric analyzer (TA Instruments). ^{1}H NMR and 13C spectra were recorded on a Bruker Avance 500 (500 MHz) spectrometer. All the electrochemical measurements were carried out using Biologic SAS VMP3 electrochemical workstation.

Electrochemical Measurements: All the electrodes were fabricated by mixing active material, acetylene black, and polyvinylidene fluoride (PVDF) in N-methyl-2-pyrrolidone (NMP) as solvent at a weight ratio of

Figure 3. a) Differential capacity plot and b) charge–discharge voltage profile of **7**, galvanostatically cycled at a current rate of C/4 in the voltage range of 1.5–3.0 V vs Na$^+$/Na. c) Voltage profile and d) cyclic stability of **8**, galvanostatically cycled at a current rate of C/4 in the voltage range of 1.5–3.0 V vs Na$^+$/Na. Inset in (c) shows the differential capacity plot for **8**.

60:30:10. The slurry was casted uniformly on stainless steel foil and the cut electrodes were dried at 65 °C in air for 6 h prior to 12 h drying at 120 °C in vacuum. Galvanostatic charge and discharge measurements on the fabricated electrodes were performed in a CR 2032 type coin cell assembled in an argon-filled glove box with moisture and oxygen level maintained at less than 0.1 ppm. 1 M $NaPF_6$ in propylene carbonate was used as the electrolyte and all the electrochemical measurements were done using Na metal as both reference and counter electrodes. The typical electrode mass loading of the active material is 1.4 mg cm^{-2}. Cyclic voltammetry was performed at a scan rate of 0.1 mV s^{-1} in a voltage range between 1.5 and 3.0 V versus Na$^+$/Na for all the derivatives. Galvanostatic charge–discharge cycling of the derivatives was carried out in the voltage range of 1.5–3.0 V versus Na$^+$/Na at a current rate of C/4.

Supporting Information

Supporting Information is available from the Wiley Online Library or from the author.

Acknowledgements

Conflict of Interest

The authors declare no conflict of interest.

Keywords

[1] S. W. Kim, D. H. Seo, X. Ma, G. Ceder, K. Kang, *Adv. Energy Mater.* **2012**, *2*, 710.
[2] H. Pan, Y. S. Hu, L. Chen, *Energy Environ. Sci.* **2013**, *6*, 2338.
[3] V. Palomares, M. Casas-Cabanas, E. Castillo-Martinez, M. H. Han, T. Rojo, *Energy Environ. Sci.* **2013**, *6*, 2312.
[4] V. Palomares, P. Serras, I. Villaluenga, K. B. Hueso, J. Carretero-Gonzalez, T. Rojo, *Energy Environ. Sci.* **2012**, *5*, 5884.
[5] J. M. Tarascon, *Nat. Chem.* **2010**, *2*, 510.
[6] J. M. Tarascon, *ChemSusChem* **2008**, *1*, 777.
[7] M. Armand, J. M. Tarascon, *Nature* **2008**, *451*, 652.
[8] S. C. Han, E. G. Bae, H. Lim, M. Pyo, *J. Power Sources* **2014**, *254*, 73.
[9] W. Deng, X. Liang, X. Wu, J. Qian, Y. Cao, X. Ai, J. Feng, H. Yang, *Sci. Rep.* **2013**, *3*, 2671.
[10] Z. Song, H. Zhan, Y. Zhou, *Angew. Chem., Int. Ed.* **2010**, *49*, 8444.
[11] Z. Song, H. Zhou, *Energy Environ. Sci.* **2013**, *6*, 2280.
[12] Z. Song, H. Zhan, Y. Zhou, *Chem. Commun.* **2009**, 448.
[13] B. Häupler, A. Wild, U. S. Schubert, *Adv. Energy Mater.* **2015**, *5*, 1402034.
[14] Y. Liang, Z. Tao, J. Chen, *Adv. Energy Mater.* **2012**, *2*, 742.
[15] G. S. Vadehra, R. P. Maloney, M. A. Garcia-Garibay, B. Dunn, *Chem. Mater.* **2014**, *26*, 7151.
[16] A. Shimizu, Y. Tsujii, H. Kuramoto, T. Nokami, Y. Inatomi, N. Hojo, J. Yoshida, *Energy Technol.* **2014**, *2*, 155.
[17] D. Tomerini, C. Gatti, C. Frayret, *Phys. Chem. Chem. Phys.* **2015**, *17*, 8604.
[18] S. Wang, L. Wang, Z. Zhu, Z. Hu, Q. Zhao, J. Chen, *Angew. Chem., Int. Ed.* **2014**, *53*, 5892.
[19] M. Armand, S. Grugeon, H. Vezin, S. Laruelle, P. Ribiere, P. Poizot, J. M. Tarascon, *Nat. Mater.* **2009**, *8*, 120.
[20] H. Chen, M. Armand, M. Courty, M. Jiang, C. P. Grey, F. Dolhem, J. M. Tarascon, P. Poizot, *J. Am. Chem. Soc.* **2009**, *131*, 8984.
[21] C. Wang, Y. Xu, Y. Fang, M. Zhou, L. Liang, S. Singh, H. Zhao, A. Schober, Y. Lei, *J. Am. Chem. Soc.* **2015**, *137*, 3124.
[22] Z. Song, Y. Qian, X. Liu, T. Zhang, Y. Zhu, H. Yu, M. Otani, H. Zhou, *Energy Environ. Sci.* **2014**, *7*, 4077.
[23] Y. Park, D.-S. Shin, S. H. Woo, N. S. Choi, K. H. Shin, S. M. Oh, K. T. Lee, S. Y. Hong, *Adv. Mater.* **2012**, *24*, 3562.
[24] K. Hernández-Burgos, S. E. Burkhardt, G. G. Rodríguez-Calero, R. G. Hennig, H. D. Abruña, *J. Phys. Chem. C* **2014**, *118*, 6046.
[25] W. Wan, H. Lee, X. Yu, C. Wang, K. W. Nam, X. Q. Yang, H. Zhou, *R. Soc. Chem. Adv.* **2014**, *4*, 19878.
[26] A. Iordache, V. Maurel, J. M. Mouesca, J. Pécaut, L. Dubois, T. Gutel, *J. Power Sources* **2014**, *267*, 553.
[27] Y. Liang, P. Zhang, S. Yang, Z. Tao, J. Chen, *Adv. Energy Mater.* **2013**, *3*, 600.
[28] Y. Liang, P. Zhang, J. Chen, *Chem. Sci.* **2013**, *4*, 1330.
[29] Y. Morita, S. Nishida, T. Murata, M. Moriguchi, A. Ueda, M. Satoh, K. Arifuku, K. Sato, T. Takui, *Nat. Mater.* **2011**, *10*, 947.
[30] S. Nishida, Y. Yamamoto, T. Takui, Y. Morita, *ChemSusChem* **2013**, *6*, 794.
[31] W. Luo, M. Allen, V. Raju, X. Ji, *Adv. Energy Mater.* **2014**, *4*, 1400554.
[32] P. Sharma, D. Damien, K. Nagarajan, M. M. Shaijumon, M. Hariharan, *J. Phys. Chem. Lett.* **2013**, *4*, 3192.
[33] S. Renault, V. A. Mihali, K. Edström, D. Brandell, *Electrochem. Commun.* **2014**, *45*, 52.
[34] S. Renault, J. Geng, F. Dolhem, P. Poizot, *Chem. Commun.* **2011**, *47*, 2414.
[35] H. Kim, J. E. Kwon, B. Lee, J. Hong, M. Lee, S. Y. Park, K. Kang, *Chem. Mater.* **2015**, *27*, 7258.
[36] K. Nagarajan, A. R. Mallia, V. S. Reddy, M. Hariharan, *J. Phys. Chem. C* 2016, 120, 8443.
[37] B. A. Jones, A. Facchetti, M. R. Wasielewski, T. J. Marks, *J. Am. Chem. Soc.* **2007**, *129*, 15259.
[38] A. J. Smith, J. R. Dahn, *J. Electrochem. Soc.* **2012**, *159*, A290.
[39] B. A. Gregg, R. A. Cormier, *J. Phys. Chem. B* **1998**, *102*, 9952.
[40] H. Banda, D. Damien, K. Nagarajan, M. Hariharan, M. M. Shaijumon, *J. Mater. Chem. A* **2015**, *3*, 10453.
[41] H. G. Wang, S. Yuan, D. I. Ma, X. I. Huang, F. I. Meng, X. B. Zhang, *Adv. Energy Mater.* **2014**, *4*, 1301651.
[42] D. Schmidt, D. Bialas, F. Würthner, *Angew. Chem., Int. Ed.* **2015**, *54*, 3611.
[43] S. Seifert, D. Schmidt, F. Wurthner, *Chem. Sci.* **2015**, *6*, 1663.
[44] R. A. Cormier, B. A. Gregg, *R. Soc. Chem. Adv.* **2014**, *4*, 2297
[45] T. Suga, S. Sugita, H. Ohshiro, K. Oyaizu, H. Nishide, *Adv. Mater.* **2011**, *23*, 751.
[46] Y. H. Wang, M. K. Hung, C. H. Lin, H. C. Lin, J. T. Lee, *Chem. Commun.* **2011**, *47*, 1249.
[47] J. Qu, T. Katsumata, M. Satoh, J. Wada, J. Igarashi, K. Mizogucho, T. Mashuda, *Chem. Eur. J.* **2007**, *13*, 7965.